Thermo-Fluid Mechanics Research Centre

School of Engineering & Applied Sciences

University of Sussex

Computation of heat transfer in a rotating cavity with a radial outflow of coolant.

Part 1: The symmetrically-heated cavity.

R.H. Rogers

July, 1985

85/TFMRC/71

Computation of heat transfer in a rotating cavity with a radial outflow of coolant.

Part 1: The symmetrically-heated cavity.

R. H. Rogers

July, 1985

85/TFMRC/71

SUMMARY

The work of Owen, Pincombe and Rogers (1985) makes use of integral momentum techniques to investigate the flow of an isothermal fluid in a rotating cavity with an imposed radial throughflow. This report extends the method by using an integral energy equation to predict the temperature in the core of the fluid when the discs of the cavity are heated, and have a given temperature distribution. The effect of various approximations are discussed, and the way in which the computed heat transfer depends on the mass-flow coefficient, the rotational Reynolds number and the type of disc-temperature distribution is found. Predictions using the theory are compared with the results of the experiments of Northrop (1984): good agreement is, in general, found.

1 Introduction

In the gas-turbine engine, temperatures are so high that cooling techniques are necessary. One situation where this arises is in the rotating discs in the engine. This report deals with the case in which two neighbouring hot discs are rotating with the same speed about a common axis, and relatively cool air is blown radially through the space between them from the axis to their outer edges. A model experiment is considered in which the two discs, each of radius b, are rotating with angular velocity Ω (see figure 1). The distance between the discs is s and each has a circular hole of radius a in the centre. It is assumed that air at temperature T_I is blown uniformly into the cavity (that is, into the space between the discs) across the cylindrical surface $r = a$, and that the rate of mass flow through this surface is $\dot{m}$. The air leaves the cavity through the cylindrical surface $r = b$. The temperatures of the discs are specified as functions of distance r from the axis.

The structure of the flow within the cavity is described by Owen, Pincombe and Rogers (1985): this paper will be referred to below as I. There is a source region ($a < r < r_e$) in which the incoming fluid is entrained into the boundary layers on the discs. For $r > r_e$, these boundary layers become nonentraining (at least when the discs are heated symmetrically about the midaxial plane of the cavity) and bear a strong resemblance to Ekman layers: for this reason they will be referred to as *Ekman-type* layers throughout this report. Finally, the fluid is redistributed from the Ekman-type layers into a sink layer near $r = b$, ready for exit from the cavity through a shroud at

$r = b$. The region between the Ekman-type layers, the source region and the sink layer is referred to as the *core*: when the discs are symmetrically heated, the radial and axial components of velocity in the core are zero; for asymmetrical heating, only the radial component is zero and there is a transfer of fluid from one disc to the other across the cavity.

Integral momentum techniques were used in I to predict the transverse component of velocity in the core, and also the thickness of the Ekman-type layers on the discs, for an isothermal cavity. In this report, the method is extended to allow for density variations in the momentum equations and to find an integral energy equation to predict the heat transfer. The method is similar to that described by Chew (1984), but there are a number of differences of detail.

In Section 2, the basic integral equations are derived under certain simplifying assumptions. The effect of these assumptions is discussed in Section 3, together with the presentation of the solutions to the equations for a number of different theoretical temperature distributions on the discs, with different flow rates through the cavity and different speeds of rotation. In Section 4, the method is applied to a number of experimental results obtained by Northrop (1984). A brief account of proposed extensions to the theory is given in Section 5.

2 Derivation of the primitive integral equations

The notation is similar to that used in I but, in view of the slight differences which are necessary in discussing the heated cavity, all quantities will be redefined here.

The axis of rotation of the discs is taken as the z-axis and the disc surfaces are $z = 0$ and $z = s$; subscripts 0 and s respectively can be used to denote values of quantities on these discs. (In fact, only the subscript 0 is used in this report, because it is assumed throughout that there is symmetry in the axial direction about the plane $z = \frac{1}{2}s$.) An overbar is used to indicate values outside the boundary layers on the discs, whether these are the entrainment layers of the source region or the Ekman-type layers bounding the core region. The subscript I is used for values appropriate to the incoming air and these values will be used as reference values where necessary. On occasion, mean values (especially of density and viscosity) are frequently used and these are denoted by the subscript m: thus

$$\rho_m = \tfrac{1}{2}(\bar{\rho} + \rho_0), \qquad \mu_m = \tfrac{1}{2}(\bar{\mu} + \mu_0). \tag{2.01}$$

The local values of all quantities have no subscript except when they are independent of z within the boundary layer: thus the local value of the mass flow rate through the boundary layer is denoted by $\dot{m}_1$.

The density of the fluid is ρ, its viscosity is μ, and its temperature is T; the pressure is p and the velocity has

components (u,v,w) in the radial, tangential and axial directions, referred to a frame of reference rotating with the discs at an angular velocity Ω about the z-axis. Cylindrical polar coordinates (r,ϕ,z) are used, with the same rotating frame of reference, and it is assumed that all the variables are independent of ϕ.

The 'thickness' of the boundary layer is denoted by δ^*: this is equivalent to saying that viscous and turbulent Reynolds stresses are negligible for $\delta^* < z < s - \delta^*$. It is assumed that, in this range, the radial component of velocity is zero: this is plausible outside the Ekman-type layers. Outside the entrainment layers, the radial component of velocity is clearly non-zero, but the assumption is consistent with the model described in I in which the entrainment layer is treated as if it were the boundary layer on a disc rotating in free space. (It is demonstrated in Appendix A that, for the symmetrically heated cavity, the thickness of the thermal boundary layer may also be assumed to be δ^*, at least for the model used in this report.)

The nondimensional parameters of the problem are the mass-flow coefficient

$$C_w = \frac{\dot{m}}{\mu_f b} \tag{2.02}$$

and the rotational Reynolds number

$$Re_\phi = \frac{\rho_f \Omega b^2}{\mu_f}. \tag{2.03}$$

The nondimensional dependent variables are

$$\delta = \frac{\rho_z}{\rho_I} \frac{\delta^*}{\delta^*_{I\,n}}, \tag{2.04}$$

where ρ_z may be taken as $\bar{\rho}$, ρ_o or ρ_m and $\delta^*_{I\,n}$ is the value of δ^* obtained by neglecting the nonlinear terms in the isothermal equations (with uniform temperature T_I);

$$V = \frac{\bar{v}}{\Omega r}; \tag{2.05}$$

$$\Upsilon = \frac{2\dot{m}_z}{\dot{m}}, \tag{2.06}$$

where $\dot{m}_z$ is the local mass-flow rate through one boundary layer (so that, when all the incoming fluid is entrained equally into the two boundary layers, $\Upsilon = 1$);

$$\theta = \frac{(T_o - \bar{T})}{T_o}; \tag{2.07}$$

$$P = \frac{\bar{p}}{\rho_I \Omega^2 b^2}. \tag{2.08}$$

The independent variable is, in the first instance,

$$x = \frac{r}{b}. \tag{2.09}$$

2.1 The equations outside the boundary layers

Since, by assumption, $\bar{u} = 0$ it follows that the equation of continuity

$$\frac{1}{r}\frac{\partial}{\partial r}(\bar{\rho}\,\bar{u}r) + \frac{\partial}{\partial z}(\bar{\rho}\,\bar{w}) = 0 \qquad (2.10)$$

gives $\bar{\rho}\,\bar{w}$ = constant. This is identically satisfied for the symmetrically-heated case since, then, $\bar{w} = 0$; however, the assumption $\bar{w} = 0$ is not made here so that the equations can be used when the theory is extended to the case of asymmetrical heating.

The radial momentum equation is

$$-\frac{\bar{\rho}\,\bar{v}^2}{r} - 2\Omega\bar{\rho}\,\bar{v} = -\frac{\partial\bar{p}}{\partial r} \qquad (2.11)$$

since $\bar{u} = 0$; this, in terms of the nondimensional variables, gives

$$\frac{\partial\bar{P}}{\partial x} = \frac{\bar{\rho}}{\rho_I}(V + 1)^2. \qquad (2.12)$$

The equations for the tangential and the axial components of momentum in the core are not used in the theory; the energy equation in the core is not used either.

2.2 The equations inside the boundary layers

It is convenient to consider first of all the axial momentum equation which, with the usual boundary layer assumptions, is

$$\frac{\partial p}{\partial z} = 0.$$

It follows that

$$p = \bar{p} = p_o, \tag{2.13}$$

and hence, using equation (2.12),

$$\frac{dP}{dx} = \frac{\bar{\rho}}{\rho_x}(V + 1)^2. \tag{2.14}$$

The equation of state is

$$p = R_a \rho T, \tag{2.15}$$

where R_a is the gas constant for air; it follows, from equation (2.13), that

$$\rho T = \bar{\rho}\bar{T} = \rho_o T_o. \tag{2.16}$$

The equation of continuity is

$$\frac{1}{r}\frac{\partial}{\partial r}(\rho u r) + \frac{\partial}{\partial z}(\rho w) = 0, \tag{2.17}$$

and it is convenient at this point to note that the local rate of mass flow within the boundary layer is

$$\dot{m}_z = 2\pi\int_0^{\delta^*} \rho u r \, dz. \tag{2.18}$$

The equations for the radial and tangential components of momentum are, respectively,

$$\frac{1}{r}\frac{\partial}{\partial r}(\rho u^2 r) + \frac{\partial}{\partial z}(\rho u w) - \frac{\rho v^2 - \bar{\rho}\,\bar{v}^2}{r} -$$

$$2\Omega(\rho v - \bar{\rho}\,\bar{v}) - \Omega^2 r(\rho - \bar{\rho}) = \frac{\partial \tau_r}{\partial z} \tag{2.19}$$

and

$$\frac{1}{r^2}\frac{\partial}{\partial r}(\rho u v r^2) + \frac{\partial}{\partial z}(\rho v w) + 2\Omega\rho u = \frac{\partial \tau_\phi}{\partial z}, \tag{2.20}$$

where τ_r and τ_ϕ are the radial and tangential components of shear stress in the fluid. The energy equation may be written as

$$\frac{1}{r}\frac{\partial}{\partial r}(r u \rho c_p T) + \frac{\partial}{\partial z}(w \rho c_p T) = -\frac{\partial q}{\partial z}, \tag{2.21}$$

where q is the heat flux in the axial direction from the disc to the fluid, and viscous dissipation is neglected (the effect of including this is discussed in Section 3.2).

2.3 The integral equations

Integration of equation (2.17) across the boundary layer on the disc $z = 0$ gives

$$\bar{\rho}\,\bar{w} = -\frac{1}{r}\frac{d}{dr}\int_0^{\delta^*} \rho u r\, dz. \qquad (2.22)$$

This equation, together with equation (2.18), gives

$$\bar{\rho}\,\bar{w} = -\frac{1}{2\pi r}\frac{d\dot{m}_z}{dr} \quad ,$$

an equation which can be derived from first principles. It is used repeatedly (and without further comment) when other equations are integrated.

Integration of equations (2.19), (2.20) and (2.21) gives

$$\frac{1}{r}\frac{d}{dr}\left(r\int_0^{\delta^*} \rho u^2 dz\right) - \frac{1}{r}\int_0^{\delta^*} (\rho v^2 - \bar{\rho}\,\bar{v}^2)\, dz -$$

$$2\Omega\int_0^{\delta^*} (\rho u - \bar{\rho}\,\bar{u})\, dz - \Omega^2 r\int_0^{\delta^*} (\rho - \bar{\rho})\, dz = -\tau_{r,o}, \qquad (2.23)$$

$$\frac{1}{r^2}\frac{d}{dr}\left(r^2\int_0^{\delta^*} \rho u v\, dz\right) - \frac{1}{2\pi}\frac{\bar{v}}{r}\frac{d\dot{m}_z}{dr} + \frac{1}{\pi}\frac{\Omega}{r}\dot{m}_z = -\tau_{\theta,o}, \qquad (2.24)$$

and

$$\frac{1}{r}\frac{d}{dr}\left(r\int_0^{\delta^*} \rho u c_p T\, dz\right) - \frac{1}{2\pi}c_p\frac{\bar{T}}{r}\frac{d\dot{m}_z}{dr} = q_o. \qquad (2.25)$$

To proceed further, it is necessary to make assumptions about the velocity and temperature profiles in the boundary layers. At this stage, a general form is assumed:

$$u = u_o f(\eta), \quad v = \bar{v} g(\eta), \quad T = T_o[1 - \theta h(\eta)], \tag{2.26}$$

where f, g and h have to be specified as functions of

$$\eta = \frac{z}{\delta^*} \tag{2.27}$$

such that

$$f(0) = g(0) = h(0) = 0 \tag{2.28}$$

and

$$f(\eta) = 0, \quad g(\eta) = h(\eta) = 1 \quad \text{when } z \geq \delta^*. \tag{2.29}$$

It is also assumed that

$$\frac{f(\eta)}{g(\eta)} \longrightarrow 1 \quad \text{as } \eta \longrightarrow 0. \tag{2.30}$$

(It should be noted that g is defined slightly differently from the form used in I: there the second of equations (2.26) was $v = \bar{v}[1 - g(\eta)]$.)

In this section it will be assumed that the variation of density through the boundary layer is negligible and ρ will be replaced by ρ_s throughout the equations; ρ_s is a function of r but not of z. The most plausible value to take for ρ_s is ρ_m as defined in equation (2.01) but, for comparison with other approaches, it is sometimes necessary to take it as $\bar{\rho}$ or ρ_o.

Using the profiles assumed in equations (2.26), it can be seen that equations (2.19), (2.23), (2.24) and (2.25) become

$$\dot{m}_1 = 2\pi I_1 \rho_1 u_o r \delta^*, \tag{2.31}$$

$$\frac{1}{r}\frac{d}{dr}(I_2 \rho_1 u_o^2 r \delta^*) + \frac{I_5}{r}\rho_1 \bar{v}^2 \delta^* + 2 I_4 \Omega \rho_1 \bar{v} \delta^* = -\tau_{r,o}, \tag{2.32}$$

$$\frac{1}{r^2 dr}(I_3 \rho_1 u_o r^2 \bar{v} \delta^*) - \frac{1}{2\pi}\frac{\bar{v}}{r}\frac{d\dot{m}_1}{dr} + \frac{1}{\pi}\frac{\Omega}{r}\dot{m}_1 = -\tau_{\phi,o}, \tag{2.33}$$

$$\frac{1}{r}\frac{d}{dr}[(I_1 - I_4)\rho_1 u_o r c_p T_o \delta^*] - \frac{1}{2\pi}\frac{c_p \bar{T}}{r}\frac{d\dot{m}_1}{dr} = q_o, \tag{2.34}$$

where

$$I_1 = \int_0^1 f(\eta)\, d\eta, \tag{2.35}$$

$$I_2 = \int_0^1 f^2(\eta)\, d\eta, \tag{2.36}$$

$$I_3 = \int_0^1 f(\eta) g(\eta)\, d\eta, \tag{2.37}$$

$$I_4 = 1 - \int_0^1 g(\eta)\, d\eta, \tag{2.38}$$

$$I_5 = 1 - \int_0^1 g^2(\eta)\, d\eta, \tag{2.39}$$

$$I_6 = \int_0^1 f(\eta) h(\eta)\, d\eta. \tag{2.40}$$

Using equation (2.31) in equations (2.32), (2.33) and (2.34), it follows that

$$\frac{r}{\rho_1 \delta^*} \frac{d(\rho_1 \delta^*)}{dr} = 2 \frac{r}{\dot{m}_1} \frac{d\dot{m}_1}{dr} - 1 + \frac{4\pi^2 I_1^2 (\rho_1 \delta^*)^2 r^4}{I_2 \dot{m}_1^2} \Omega^2 \left[I_5 \left(\frac{\bar{v}}{\Omega r} \right)^2 + 2 I_4 \frac{\bar{v}}{\Omega r} \right] + \frac{4\pi^2 I_1^2 \rho_1 \delta^* r^3}{I_2} \tau_{r,o}, \tag{2.41}$$

$$\frac{r}{\bar{v}} \frac{d\bar{v}}{dr} = \left(\frac{I_1}{I_3} - 1 \right) \frac{r}{\dot{m}_1} \frac{d\dot{m}_1}{dr} - 1 - \frac{2 I_1}{I_3} \frac{\Omega r}{\bar{v}} - \frac{2\pi I_1 r}{I_3 \dot{m}_1 \Omega} \frac{\Omega r}{\bar{v}} \tau_{\phi,o}, \tag{2.42}$$

$$r \frac{d\theta}{dr} = \left(\frac{I_1}{I_4} - 1 \right) \theta \frac{r}{\dot{m}_1} \frac{d\dot{m}_1}{dr} + \left(\frac{I_1}{I_4} - \theta \right) \frac{r}{T_o} \frac{dT_o}{dr} - \frac{2\pi I_1 r^2}{I_4 \dot{m}_1 c_p T_o} q_o. \tag{2.43}$$

2.4 The tangential stresses and the heat flux at the disc

It is convenient, first, to express $\tau_{r,o}$ and q_o in terms of $\tau_{\phi,o}$. It will be assumed that, near the disc, the ratio of the radial and transverse components of stress is equal to the ratio of the radial and transverse components of the fluid velocity relative to the rotating disc (see, for example, von Kármán (1921)). Then, using the relation (2.30),

$$\tau_{r,o} = \frac{u_o}{\bar{v}}\,\tau_{\phi,o} = \frac{\dot{m}_i}{2\pi\rho_i \bar{v}\delta^* r I_1}. \qquad (2.44)$$

The Reynolds analogy for a rotating disc is assumed to hold for the heat transfer; at this stage dissipation is neglected, so that

$$\frac{q_o}{c_p} = \chi\,\frac{T_o - \bar{T}}{\bar{v}}\,\tau_{\phi,o}, \qquad (2.45)$$

where χ is a factor depending on the Prandtl number Pr. When $Pr = 1$ the value of χ is unity; its dependence on Pr is discussed in Section 3.4.

It is convenient to express equations (2.41) to (2.43) in nondimensional form using the definitions (2.2) to (2.7), together with the solution to the isothermal "linear" equations; in these the inertial terms in equations (2.19) and (2.20) are negligible compared with the Coriolis terms, the radial mass flow is divided equally between the two boundary layers (so that $\Upsilon = 1$) and the density is assumed constant with $\rho = \rho_i$ throughout the boundary layer. (This solution has already been referred to in the definition of δ.)

The equations then become

$$\frac{x}{\delta}\frac{d\delta}{dx} = B_1\frac{x}{\Upsilon}\frac{d\Upsilon}{dx} + B_2 + B_3\frac{\Psi}{\Upsilon V} + (B_4 v^2 + B_5 V)\left(\frac{\delta}{\Upsilon V_{i,in}}\right)^2, \qquad (2.46)$$

$$\frac{x}{V}\frac{dV}{dx} = B_7\frac{x}{\gamma}\frac{d\gamma}{dx} + B_8 + B_9\frac{1}{V} + B_{10}\frac{\Psi}{\gamma V}, \tag{2.47}$$

$$x\frac{d\theta}{dx} = B_{11}\frac{x}{\gamma}\frac{d\gamma}{dx} + B_{12}\frac{x}{T_o}\frac{dT_o}{dx} + B_{13}\frac{\Psi}{\gamma V}\theta, \tag{2.48}$$

where

$$\Psi = \frac{\tau_{\phi,o}}{(\tau_{\phi,o})_{flat}} \tag{2.49}$$

and the coefficients B_k are given in the first column of Table 1. In this form, the equations may be used for any choice of profiles for the velocity and temperature.

2.5 Choice of the velocity and temperature profiles

In this report, computations for turbulent flow are presented with velocity profiles which are generalizations of those used by von Kármán (1921); they are the same as those used in I, and are given by

$$f(\eta) = \eta^{1/n}(1 - \eta) \tag{2.50}$$

and

$$g(\eta) = \eta^{1/n}, \tag{2.51}$$

where n is usually taken as 7. Furthermore, it will be assumed that the temperature profile is similar to the profile of the tangential component of velocity: this gives

$$h(\eta) = \eta^{1/n}. \tag{2.52}$$

This is strictly valid only when $Pr = 1$, T_I is constant, and $T_o - T_I \propto r^2$. For integral momentum methods, however, the *exact* form of the profile is assumed to be unimportant; Chew (1984) has found solutions which do not make this assumption, and his results are discussed in Section 3.3.

It is assumed, as in I and by analogy with von Kármán's solution, that

$$\tau_{w,o} = K_n^2 \rho_I \left(\frac{\mu_I}{\rho_I \delta^{**}}\right)^{2\alpha-3} \overline{v}(u_o^2 + \overline{v}^2)^{2-\alpha}, \tag{2.53}$$

where

$$\alpha = \frac{3n + 5}{2(n + 1)}, \tag{2.54}$$

so that $\alpha = 1.625$ when $n = 7$. It is shown in I that, with these assumptions,

$$\delta_{I,n}^{**} = P_n |C_w|^{2-\alpha} Re_\delta^{-1/4} x^{\alpha-2} \tag{2.55}$$

and

$$V_{I,n} = -\lambda_o x^{-\alpha}, \tag{2.56}$$

where

$$\lambda_o = \mathrm{sgn}(C_w)\, P_n' |C_w|^{\alpha-1} Re_\delta^{-1/4}. \tag{2.57}$$

The constants K_n, P_n and P_n' are tabulated for $n = 5, 6, 7, 8, 9$ in Table 4 of I; in particular (for the

case discussed here),

$$K_7^2 = 0.0225, \quad P_7 = 0.159, \quad P_7' = 2.22. \tag{2.58}$$

Using these expressions in the definition (2.49), it may be shown that

$$\Psi = \frac{\rho_I}{\rho_I}\left(\frac{\mu_I}{\mu_I}\right)^{2\alpha-3} \frac{V|\gamma|^{4-2\alpha}}{V_{I,in}\delta}\left(\frac{I_4}{I_1 + I_4}\right)^{2-\alpha}\left[1 + \frac{I_1}{I_4}\left(\frac{\delta V}{\gamma V_{I,in}}\right)^2\right]^{2-\alpha}. \tag{2.59}$$

2.6 The expression for the Nusselt number

The nondimensional measures of the heat transfer from the disc are the local Nusselt number

$$Nu = \frac{rq_o}{k_I(T_o - T_I)} \tag{2.60}$$

and the average Nusselt number

$$Nu_{av} = \frac{bq_{o,av}}{k_I(T_o - T_I)_{av}}, \tag{2.61}$$

where k is the thermal conductivity of the air,

$$q_{o,av} = \frac{2}{b^2 - a^2}\int_a^b rq_o dr \tag{2.62}$$

and

$$(T_o - T_r)_{av} = \frac{2}{b^2 - a^2}\int_a^b r(T_o - T_r)\,dr. \qquad (2.63)$$

It would be more natural to use k_s instead of k_r in the definitions (2.60) and (2.61), but k_r was used for the experimental results available and is used here to make comparisons easier; it is not expected that the value of Nu will be significantly affected by this.

A more serious defect of the definitions is the use of the temperature difference $T_o - T_r$ in the denominator. It would be more appropriate to replace T_r by $\bar{T}$, but $\bar{T}$ is not known in the experiments and T_r is the only reference temperature available. Furthermore, as Chew (1984) has pointed out, T_o should be replaced by the adiabatic wall temperature which will be discussed more fully in Section 3.2; the present form is regained, however, to facilitate comparison with the experimental results. The effect of this is substantial at high values of the rotational Reynolds number.

Using the definition (2.45), and expressing the result in terms of the nondimensional variables, it may be seen that

$$\frac{rq_o}{k_r} = -\frac{1}{2\pi} Pr\, \chi\, C_w \frac{T_o \Psi\theta}{xV}, \qquad (2.64)$$

since, using equation (2.24) without the nonlinear terms, and with $\gamma = 1$,

$$\left(\frac{\tau_{\phi,0}}{\rho_\infty \Omega^2 b^2}\right)_{lin} = -\frac{1}{2\pi x} C_w Re_\phi^{-1}. \qquad (2.65)$$

3 Solutions to various corrected forms of the primitive equations

In the derivation of equations (2.46) to (2.48), it was assumed that the density variation across the boundary layer is negligible, that viscous dissipation can be neglected in the energy equation and that the temperature variation on the disc is quadratic. Also the form of the necessary correction due to the fact that $Pr \neq 1$ was not discussed. These effects will be discussed below and their importance estimated by comparing the solutions for a number of cases.

Most computations were carried out with a = 42.75 mm, b = 427.5 mm and T_∞ = 30°C. Values of C_w = 1 400 and 14 000, of $Re_\phi = 10^5$ and 3×10^6, and of Pr = 1 and 0.71 were used. Three temperature distributions on the disc were considered; these were $T_0 = T_\infty + 70°x^2$, $T_\infty + 45°$, and $T_\infty + 14°/x$. The local Nusselt number Nu was computed and, in all cases, the graphs show Nu as a function of x; in one case, the value of Nu_{av} is also shown as a function of Re_ϕ for various values of C_w and various distributions of T_0.

In the ensuing discussion, x will be retained as the independent variable; for computational purposes, it was convenient to use, instead,

$$\xi = \frac{x^{\alpha}}{\lambda_o}, \qquad (3.01)$$

where λ_o is defined in equation (2.56). Clearly, with the distributions discussed in Section 2.4, $V_{max} = -1/\xi$ (as in I). The transformation is easy to perform since, for any dependent variable F,

$$\frac{dF}{d\xi} = \frac{x}{\alpha\xi}\frac{dF}{dx}.$$

The computations were started at $x = a/b$ which was assumed to be in the entrainment layer. The model described in I is used for this layer, so that $V = -1$ and Υ is unknown. Hence equation (2.47) has to be rearranged to give an expression for $d\Upsilon/dx$. Equations (2.46) and (2.47), together with suitable starting values, can be regarded as an initial value problem for δ and Υ and a variable-step Gear method can be used to solve them. The starting values used for the computations were $\delta = 10^{-4}$ and $\Upsilon = 4\times10^{-7}$; it was found that the solution was insensitive to smaller values than this. Outside the entrainment layer it was assumed that the temperature was constant so that $\overline{T} = T_I$ (see Appendix A) and there was no need to use equation (2.48) in this region.

The computation was continued with increasing x until Υ had increased to the value unity. For values of x greater than this, equations (2.46) to (2.48) were used with $d\Upsilon/dx = 0$ to find δ, V and θ as functions of x outside the Ekman-type layer. The starting values for this part of the computation were found by assuming that δ, V and θ were continuous in the transition from the entrainment layer to the Ekman-type layer.

3.1 The effect of variable density within the boundary layer

When the density is not assumed independent of z in equations (2.23) to (2.25), integrals of the form

$$J_0(\theta) = \frac{1}{1-\theta} - \int_0^1 \frac{1}{1-\theta h(\eta)}\, d\eta, \tag{3.02}$$

$$J_1(\theta) = \int_0^1 \frac{f(\eta)}{1-\theta h(\eta)}\, d\eta, \tag{3.03}$$

$$J_2(\theta) = \int_0^1 \frac{f^2(\eta)}{1-\theta h(\eta)}\, d\eta, \tag{3.04}$$

$$J_3(\theta) = \int_0^1 \frac{f(\eta)g(\eta)}{1-\theta h(\eta)}\, d\eta, \tag{3.05}$$

$$J_4(\theta) = \frac{1}{1-\theta} - \int_0^1 \frac{g(\eta)}{1-\theta h(\eta)}\, d\eta, \tag{3.06}$$

and

$$J_5(\theta) = \frac{1}{1-\theta} - \int_0^1 \frac{g^2(\eta)}{1-\theta h(\eta)}\, d\eta \tag{3.07}$$

arise instead of the integrals I_k defined in equations (2.35) to (2.40). (It may be noted that $J_0(0) = 0$, $J_k(0) = I_k$ for $k = 1$ to 5 and $J_1'(0) = I_6$.) Equations (2.46) to (2.48) are still valid, but the coefficients are now those given in the last column of Table 1.

Figure 2 shows comparisons between the solution using this correction with those using the primitive equations. (The method used to compute the coefficients B_k is given in Appendix B.) It can be seen from the graphs that the difference between the two solutions is very small; this is in spite of the fact that the values of the coefficients vary considerably: a set of values of the coefficients using the two approaches is given, for a typical run, in Table 2. The computation, using the correction, takes about 10 times as long as that for the primitive equations; it is therefore considered that it is not worth including this correction for any prediction of Nusselt numbers.

3.2 The effect of viscous dissipation when $Pr = 1$

It has been shown by Owen (1971) that, for a free disc, it is appropriate to use a "total enthalpy" in the Reynolds analogy rather than the temperature. For the present problem, the discussion in Section 2 above needs to be modified as described below.

The total enthalpy is defined as

$$H = c_p T + \tfrac{1}{2}[u^2 + (v + \Omega r)^2], \qquad (3.08)$$

and equation (2.21) is replaced by

$$\frac{1}{r}\frac{\partial}{\partial r}(\rho u r H) + \frac{\partial}{\partial z}(\rho w H) = -\frac{\partial}{\partial z}[q - u\tau_r - (v + \Omega r)\tau_\theta]. \qquad (3.09)$$

Equation (2.25) becomes

$$\frac{1}{r}\frac{d}{dr}\left(r\int_0^{\delta^*}\rho u H\,dz\right) - \frac{1}{2\pi}\frac{\overline{H}}{r}\frac{d\dot{m}_i}{dr} = q_o - \Omega r \tau_{\phi,o}, \qquad (3.10)$$

and the third of equations (2.26) is now

$$H = H_o[1 - \theta h(\eta)], \qquad (3.11)$$

so that, now,

$$\theta = \frac{H_o - \overline{H}}{H_o}.$$

The Reynolds analogy (2.45) becomes

$$q_o - \Omega r \tau_{\phi,o} = \frac{H_o - \overline{H}}{\overline{v}}\tau_{\phi,o} \qquad (3.12)$$

where the factor χ has been omitted since, in this section, $Pr = 1$. It follows that equations (2.46) and (2.47) are unchanged and that, in equation (2.48), the term $\frac{x}{T_o}\frac{dT_o}{dx}$ is replaced by $\frac{x}{H_o}\frac{dH_o}{dx}$.

Comparisons of solutions obtained using this correction and without it are shown in figure 3. For small rotations the effect is negligible but, as might be expected, the effect increases with Re_ϕ and is certainly significant for large values of this parameter. Throughout the rest of this report, the effect of viscous dissipation will be included in the equations.

3.3 The effect of the temperature distribution on the disc ($Pr = 1$)

Chew (1984) has extended the work of Dorfman (1963) who discussed the effect of the temperature distribution on a disc rotating in free space. When $Pr = 1$, Chew assumes that the local Nusselt number

$$Nu \propto x^2 Re_\phi (Re_T^*)^\beta, \tag{3.13}$$

where (using the notation of this report)

$$Re_T^* = (I_1 - I_\phi) \frac{\rho_s \delta^* (u_o^2 + \bar{v}^2)}{\mu^2} \tag{3.14}$$

and $\beta = 2\alpha - 3$ for the special distributions of f and g discussed in Section 2.5 above. He makes no assumption about the distribution of h but uses the Reynolds analogy (2.45) together with equation (2.48) to obtain a differential equation for I_ϕ. (Chew also considers the effect of varying Pr, but his method is not presented in this report.)

A comparison of the two methods (with $\rho_s = \bar{\rho}$) is shown in figure 4. As is to be expected, the results are indistinguishable when $T_o = T_s + 70x^2$, but there is a noticeable difference for other temperature distributions. It should be noticed, however, that both methods give maximum values of Nu at approximately the same value of x, and the same applies to zero values of Nu. Thus the correction has the effect of requiring a multiplicative factor on the value of Nu; this is hardly surprising in view of the nature of the assumption made by the use of equation (3.13).

Whether Chew's assumption is superior to that of this report (where it is assumed that $h = f$) can only be determined by comparison with experiment. This will be considered in Section 4 below.

3.4 The effect of varying Prandtl number

In terms of temperature, equation (3.12) gives

$$q_0 = \frac{c_p(T_0 - \bar{T}) - \tfrac{1}{2}\bar{v}^2}{\bar{v}}\tau_{\phi,0}$$

when dissipation is included in the energy equation and $Pr = 1$. This gives an adiabatic wall temperature

$$T_{0,ad} = \bar{T} + \frac{\bar{v}^2}{2c_p}.$$

When $Pr \neq 1$, a correction factor R is used and the adiabatic wall temperature is written as

$$T_{0,ad} = \bar{T} + R\frac{\bar{v}^2}{2c_p}, \qquad (3.15)$$

where R is a function of Pr. For the flow over a flat plate, Rotta (1964) gives an expression for R which, when modified for a rotating disc, may be written as

$$R = 1 + 94.75\,Pr^{-0.4}\,(Pr - 1)\,\frac{\tau_{\phi,0}}{\rho_f\Omega^2 b^2}, \qquad (3.16)$$

where the coefficient $94.75Pr^{-0.4}$ is obtained (as an approximation) by interpolation from Table 23.1 given by

Schlichting (1979). Many authors, according to Schlichting, take

$$R = Pr^{\frac{1}{3}} \tag{3.17}$$

for turbulent flow. A comparison of this approximate value of R with values found using equation (3.16) is shown in Table 3 for several values of $\frac{\tau_{\phi,o}}{\rho_f \Omega^2 b^2}$.

When dissipation effects are neglected, the work of Dorfman (1964) gives the expression for the function χ introduced in equation (2.45) from

$$\frac{1}{\chi} = 1 + 5\{Pr - 1 + \log_e[(5Pr + 1)/6]\} \sqrt{(\tau_{\phi,o}/\rho_f \Omega^2 b^2)}. \tag{3.18}$$

(This is identical with the result of von Kármán (1939) for a flat plate.) A commonly used approximation is

$$\chi = Pr^{-0.4}, \tag{3.19}$$

and a comparison between the two expressions is given in Table 3.

Figure 5 shows comparisons between the solutions, with $Pr = 0.71$, using equations (3.16) and (3.18) and those using equations (3.17) and (3.19). For some reason not yet understood, the computations failed when equations (3.16) and (3.18) were used with $C_w = 1\ 400$, $Re_\phi = 3 \times 10^6$; the graph for this case, therefore, includes curves for the approximate equations only. It is clear that use of the approximate form (whenever

both solutions are possible) causes little error and reduces computational time. It is suggested, therefore, that equations (3.17) and (3.19) should be used for R and for χ.

3.5 The average Nusselt number

Figure 6 shows predictions of the variation of $Nu_{\phi,v}$ with Re_ϕ for three values of C_w and for increasing, constant and decreasing disc-temperature distributions. The graphs are in good agreement with similar curves presented by Chew (1984). The fall-off for large values of Re_ϕ is due to the use of $(T_o - T_f)_{\phi,v}$, instead of $(T_{o,\phi} - \overline{T})_{\phi,v}$ in the expression for $Nu_{\phi,v}$, as described in Section 2.6; the sharpness of the fall-off is remarkable.

4 Comparison with experiment

The computations for comparison with the experiments of Northrop (1984) were made using the approximate equations (3.17) and (3.19). The comparisons presented here are with the experimentally measured heat fluxes using fluxmeters. (A comparison with the computed heat fluxes using the so-called "conduction solution" is discussed by Long (1985).)

The disc-temperature distributions used in the computations were computed using a faired spline technique on the measured values. In the experiments, disc temperatures were not measured for $x < 0.2$, whereas the computations were started at $x = 0.1$; it was assumed that, when $x = 0.1$, $T_o = T_f$ and

a quadratic was fitted to the cubic spline for $0.1 < x < 0.2$. The solution for $x > 0.15$ was independent of the starting values chosen.

Figure 7 shows a comparison between theory and experiment for disc temperatures which increased with radius, for various values of Re_ϕ and for C_w = 1 400; Figures 8 and 9 show similar comparisons for C_w = 7 000 and C_w = 14 000 respectively. The agreement is, in general good, except occasionally for small values of x where the model used for the source region does not bear much relation to the experiment. This is particularly evident when C_w is large and Re_ϕ is small, so that the source region occupies most of the cavity.

Figure 10a shows comparisons between the theory presented here and that of Chew (1984) for the downstream disc with C_w = 7 000, three values of Re_ϕ and different disc temperature distributions. Figure 10b shows similar comparisons for the upstream disc. In general, both sets of theoretical curves show good agreement with the experimental results, but Chew's predictions are rather better than those of this report in the source region, and also for the Ekman-type layer when the source region occupies most of the cavity (the smallest values of Re_ϕ). Even here, however, the errors of the present theory are small considering the inadequacy of the model in the source region, as well as experimental error in the flux meter readings.

It would appear from these graphs that the present theory is adequate (except, possibly, for low values of Re_ϕ) for the prediction of Nusselt numbers even though no correction has been

made for the nonquadratic temperature distributions which occur. The method used has the advantage of simplicity over that of Chew.

5 Conclusions

It has been shown that the integral technique used for the momentum equations in I can be usefully extended to find temperature distributions and, hence, heat transfer from the discs of a symmetrically-heated rotating cavity. It is concluded that, in the momentum equations, it is sufficient to neglect the variation of density across the boundary layers on the disc; that it is necessary, especially at high rotational Reynolds numbers, to include the effect of dissipation in the energy equation; that it is possible to ignore the effect of nonquadratic disc-temperature distributions on the Reynolds analogy, at least to a fair degree of accuracy; and that approximate expressions may be used for the factors introduced to allow for a Prandtl number not equal to unity.

Comparison with experiment over wide ranges of the parameters C_w and Re_ϕ, and for several disc-temperature distributions show good agreement.

One of the basic inadequacies of the model used for the source region is that it is assumed that the radial component of velocity outside the entrainment layer is zero; this is clearly not the case. An extension to the theory would be possible to allow for this but, in view of the generally good

agreement obtained with the present model, investigation of this effect is not a matter of urgency.

The probability that the flow in the source region outside the entrainment layer is a free vortex (rather than having zero rotation, as has been assumed in all the computations presented here) can easily be allowed for since $v_\bullet$ has to be specified in the computations. Preliminary runs have shown that, for a/b = 0.1, there is little difference between the two cases.

An extension of the theory to the nonsymmetrical case is obviously important, and so is its adaptation to the case of inflow. It is planned to proceed further in both these directions.

Acknowledgements

The author wishes to thank Dr J. W. Chew for supplying copies of his computer output for the comparisons presented in this report. She also wishes to thank him and Dr J. M. Owen for their help in the many discussions held while the work was in progress. She is grateful to the SERC, to Rolls Royce Limited and to GEC Ruston Gas Turbines Limited for their financial support for the work.

References

Chew, J.W. 1983 The effect of frictional heating and compressive work in rotating axisymmetric flow.
Report TSG0154, Rolls Royce, Derby.

Chew, J.W. 1984 An integral method for the calculation of flow and heat transfer in a symmetrically heated rotating cavity.
Report TSG0155, Rolls Royce, Derby.

Dorfman, L.A. 1963 Hydrodynamic resistance and the heat loss of rotating solids.
Oliver and Boyd, Edinburgh and London.

Kármán, Th. von 1921 Uber laminare und turbulente Reibung.
Z.angew.Math.Mech., 1, 233.

Kármán, Th. von 1939 The analogy between fluid friction and heat transfer.
Trans.ASME, 61, 705.

Long, C. A. 1985 Transient analysis of experimental data from the Mark 2 rotating cavity rig.
Report 85/TFMRC/76, School of Engineering and Applied Sciences, University of Sussex.

Northrop, A. 1984 Heat transfer in a cylindrical rotating cavity.
D.Phil. thesis, University of Sussex.

Owen, J. M. 1971 The Reynolds analogy applied to flow between a rotating and a stationary disc.
Int.J.Heat and Mass Transfer, 14, 451.

Owen, J. M., Pincombe, J. R. and Rogers, R. H. 1985 Source-sink flow inside a rotating cylindrical cavity.
J.Fluid Mech., 135, 233.

Rogers, R. H. 1959 The structure of the jet-stream in a rotating fluid with a horizontal temperature gradient.
J.Fluid Mech., 5, 41.

Rotta, J. C. 1964 Temperaturverteilungen in der turbulenten Grenzschicht an der ebenen Platte.
Int.J.Heat Mass Transfer, 7, 215.

Schlichting, H. 1979 Boundary-Layer Theory.
McGraw-Hill Book Company (London)

k	Approximate equations		Full equations
	General	$n = \frac{1}{7}$	
1	2	2	$2 + \left(\frac{J_2'(\theta)}{J_2(\theta)} - \frac{2J_1'(\theta)}{J_1(\theta)}\right)B_{11}$
2	$1 - \alpha$	-0.625	$1 - \alpha + \left(\frac{J_2'(\theta)}{J_2(\theta)} - \frac{2J_1'(\theta)}{J_1(\theta)}\right)B_{12}\frac{x}{T_o}\frac{dT_o}{dx}$
3	$-\frac{2I_1}{I_2}$	-3.94	$-\frac{2J_1(\theta)}{J_2(\theta)} + \left(\frac{J_2'(\theta)}{J_2(\theta)} - \frac{2J_1'(\theta)}{J_1(\theta)}\right)B_{13}\theta$
4	$\frac{I_1 I_5}{I_2 I_4}$	3.50	$\frac{J_1^2(\theta)J_5(\theta)}{J_1(0)J_4(0)J_2(\theta)}$
5	$\frac{2I_1}{I_2}$	3.94	$\frac{2J_1^2(\theta)J_4(\theta)}{J_1(0)J_4(0)J_2(\theta)}$
6	0	0	$\frac{J_1^2(\theta)J_0(\theta)}{J_1(0)J_4(0)J_2(\theta)}$
7	$\frac{I_1}{I_3} - 1$	0.2	$\frac{J_1(\theta)}{J_3(\theta)} - 1 + \left(\frac{J_1'(\theta)}{J_1(\theta)} - \frac{J_3'(\theta)}{J_3(\theta)}\right)B_{11}$
8	-2	-2	$-2 + \left(\frac{J_1'(\theta)}{J_1(\theta)} - \frac{J_3'(\theta)}{J_3(\theta)}\right)B_{12}\frac{x}{T_o}\frac{dT_o}{dx}$
9	$-\frac{2I_1}{I_3}$	-2.4	$-\frac{2J_1(\theta)}{J_3(\theta)}$
10	$\frac{2I_1}{I_3}$	2.4	$\frac{2J_1(\theta)}{J_3(\theta)} + \left(\frac{J_1'(\theta)}{J_1(\theta)} - \frac{J_3'(\theta)}{J_3(\theta)}\right)B_{13}\theta$
11	$\left(\frac{I_1}{I_6} - 1\right)\theta$	0.2θ	$\frac{J_1(\theta)}{J_1'(\theta)}\left(1 - (1-\theta)\frac{J_1(\theta)}{J_1(0)}\right)$
12	$\frac{I_1}{I_6} - \theta$	$1.2 - \theta$	$\frac{J_1(\theta)}{J_1'(\theta)}$
13	$\frac{2I_1}{I_6}X$	$2.4X$	$\frac{2J_1^2(\theta)}{J_1(0)J_1'(\theta)}X$

Table 1 The coefficients B_k in the integral equations

Note: in B_2, $\alpha = -\frac{x}{V_{isn}}\frac{dV_{isn}}{dx}$

(a)

x	B_1	B_2	B_3	B_4	B_5	B_6	B_7	B_8	B_9	B_{10}	B_{11}	B_{12}	B_{13}
0.1	2.000	-0.625	-3.943	3.505	3.943	0.000	0.200	-2.000	-2.400	2.400	0.063	0.884	2.400
0.15	2.000	-0.625	-3.943	3.505	3.943	0.000	0.200	-2.000	-2.400	2.400	0.047	0.964	2.400
0.2	2.000	-0.625	-3.943	3.505	3.943	0.000	0.200	-2.000	-2.400	2.400	0.038	1.012	2.400
0.25	2.000	-0.625	-3.943	3.505	3.943	0.000	0.200	-2.000	-2.400	2.400	0.031	1.043	2.400
0.3	2.000	-0.625	-3.943	3.505	3.943	0.000	0.200	-2.000	-2.400	2.400	0.027	1.065	2.400
0.35	2.000	-0.625	-3.943	3.505	3.943	0.000	0.200	-2.000	-2.400	2.400	0.024	1.081	2.400
0.4	2.000	-0.625	-3.943	3.505	3.943	0.000	0.200	-2.000	-2.400	2.400	0.021	1.094	2.400
0.45	2.000	-0.625	-3.943	3.505	3.943	0.000	0.200	-2.000	-2.400	2.400	0.019	1.103	2.400
0.5	2.000	-0.625	-3.943	3.505	3.943	0.000	0.200	-2.000	-2.400	2.400	0.018	1.111	2.400
0.55	2.000	-0.625	-3.943	3.505	3.943	0.000	0.200	-2.000	-2.400	2.400	0.017	1.117	2.400
0.6	2.000	-0.625	-3.943	3.505	3.943	0.000	0.200	-2.000	-2.400	2.400	0.014	1.129	2.400
0.65	2.000	-0.625	-3.943	3.505	3.943	0.000	0.200	-2.000	-2.400	2.400	0.012	1.140	2.400
0.7	2.000	-0.625	-3.943	3.505	3.943	0.000	0.200	-2.000	-2.400	2.400	0.010	1.150	2.400
0.75	2.000	-0.625	-3.943	3.505	3.943	0.000	0.200	-2.000	-2.400	2.400	0.008	1.158	2.400
0.8	2.000	-0.625	-3.943	3.505	3.943	0.000	0.200	-2.000	-2.400	2.400	0.007	1.165	2.400
0.85	2.000	-0.625	-3.943	3.505	3.943	0.000	0.200	-2.000	-2.400	2.400	0.006	1.170	2.400
0.9	2.000	-0.625	-3.943	3.505	3.943	0.000	0.200	-2.000	-2.400	2.400	0.005	1.174	2.400
0.95	2.000	-0.625	-3.943	3.505	3.943	0.000	0.200	-2.000	-2.400	2.400	0.005	1.177	2.400
1.0	2.000	-0.625	-3.943	3.505	3.943	0.000	0.200	-2.000	-2.400	2.400	0.004	1.179	2.400

(b)

x	B_1	B_2	B_3	B_4	B_5	B_6	B_7	B_8	B_9	B_{10}	B_{11}	B_{12}	B_{13}
0.1	1.928	-0.298	-4.873	8.088	10.526	1.663	0.192	-1.994	-2.387	2.369	0.061	0.871	2.369
0.15	1.950	-0.383	-4.575	6.336	7.929	0.934	0.194	-1.996	-2.391	2.379	0.046	0.955	2.379
0.2	1.962	-0.433	-4.423	5.548	6.789	0.639	0.196	-1.997	-2.393	2.385	0.037	1.005	2.385
0.25	1.969	-0.467	-4.330	5.105	6.157	0.483	0.197	-1.997	-2.394	2.388	0.031	1.037	2.388
0.3	1.974	-0.491	-4.269	4.823	5.758	0.388	0.197	-1.998	-2.395	2.390	0.027	1.060	2.390
0.35	1.978	-0.510	-4.225	4.629	5.486	0.325	0.197	-1.998	-2.396	2.391	0.023	1.077	2.391
0.4	1.980	-0.525	-4.193	4.489	5.290	0.281	0.198	-1.998	-2.396	2.392	0.021	1.090	2.392
0.45	1.982	-0.537	-4.168	4.384	5.144	0.248	0.198	-1.999	-2.397	2.393	0.019	1.100	2.393
0.5	1.984	-0.548	-4.149	4.303	5.033	0.224	0.198	-1.999	-2.397	2.394	0.018	1.108	2.394
0.55	1.987	-0.558	-4.133	4.240	4.946	0.205	0.198	-1.999	-2.397	2.394	0.016	1.114	2.394
0.6	1.987	-0.566	-4.104	4.120	4.780	0.169	0.199	-1.999	-2.398	2.395	0.014	1.127	2.395
0.65	1.989	-0.574	-4.077	4.013	4.633	0.138	0.199	-1.999	-2.398	2.396	0.012	1.138	2.396
0.7	1.991	-0.581	-4.054	3.923	4.509	0.112	0.199	-1.999	-2.398	2.397	0.010	1.148	2.397
0.75	1.993	-0.588	-4.035	3.848	4.408	0.092	0.199	-1.999	-2.399	2.397	0.008	1.157	2.397
0.8	1.994	-0.595	-4.019	3.789	4.327	0.075	0.199	-2.000	-2.399	2.398	0.007	1.164	2.398
0.85	1.995	-0.602	-4.007	3.743	4.265	0.063	0.199	-2.000	-2.399	2.398	0.006	1.170	2.398
0.9	1.996	-0.608	-3.998	3.709	4.219	0.054	0.199	-2.000	-2.399	2.398	0.005	1.174	2.398
0.95	1.996	-0.614	-3.992	3.685	4.186	0.047	0.200	-2.000	-2.399	2.398	0.004	1.177	2.398
1.0	1.996	-0.620	-3.988	3.669	4.165	0.043	0.200	-2.000	-2.399	2.399	0.004	1.179	2.399

Table 2 The coefficients B_k using
(a) the primitive equations, and
(b) the method of Section 3.1.

[C_w = 14000, $Re_\delta = 3x10^6$ and $T_o = T_r + 14/x$]

$\frac{\tau_{\phi,0}}{\rho_f \Omega^2 b^2}$	R	X
	eqn. (3.16)	eqn. (3.18)
0.001	0.9685	1.0984
0.002	0.9370	1.1451
0.003	0.9055	1.1837
0.004	0.8740	1.2183
Approx. value	eqn. (3.17) 0.892	eqn. (3.19) 1.1468

Table 3 The correction factors R and X defined in Section 3.4, $Pr = 0.71$.

[For a free disc, $\frac{\tau_{\phi,0}}{\rho_f \Omega^2 b^2}$ varies from 4.2×10^{-3} when $x^2 Re_\phi = 10^4$ to 1.1×10^{-3} when $x^2 Re_\phi = 10^7$.]

Appendix A The thickness of the thermal boundary layer

It is well known (see, for example, Schlichting (1979)) that, for the flow of a fluid over a heated flat plate, the thermal boundary layer is thicker (when $Pr < 1$) than the momentum boundary layer.

For an Ekman layer on a heated rotating flat plate, Chew (1983) has pointed out that the thermal boundary layer may be as much as an order of magnitude thicker than the momentum layer. This result was also noticed by Rogers (1959) for a water-filled cavity whose axis was vertical and which had an applied horizontal temperature gradient. The result is independent of Prandtl number over a wide range of values, both for $Pr < 1$ and for $Pr > 1$.

The present case of a cavity bounded by two discs whose temperature distributions are identical is an exception to the general results described above. Outside the Ekman-type layer (which is a momentum boundary layer), it is assumed that $u = w = 0$ for $z > \delta^*$. If the thickness of the thermal boundary layer is denoted by δ_T^*, and it is assumed that $\delta_T^* > \delta^*$, it follows that $u = w = 0$ for $\delta^* < z < \delta_T^*$; inspection of equation (2.21) shows immediately that $\frac{\partial q}{\partial z} = 0$ for $\delta^* < z < \delta_T^*$. A similar argument applies to the disc $z = s$ and so, since there is symmetry about $z = \frac{1}{2}s$, $q = 0$ in this region. It follows that all the temperature variation is within the momentum boundary layer. This is equivalent to saying that $\delta^* = \delta_T^*$ for the Ekman-type layer.

This argument does not apply to the entrainment layer. However, the fluid outside this layer (which is a momentum boundary layer) originates entirely from the source; since the flow is inviscid, its temperature (or more precisely, its total enthalpy) is unchanged from the inlet value. There is, therefore, no need to use the energy equation in the source region to determine $\overline{T}$, and the value of δ_T^{**} is irrelevant.

Appendix B Evaluation of the integrals $J_k(\theta)$

The integrals defined in equations (3.02) to (3.07), together with their derivatives, have to be evaluated for every value of θ for which they are used. For the particular functions defined in equations (2.50) to (2.52), it is possible to find an analytic form since it may be shown that

$$\int_0^1 \frac{\eta^{k+j/n}}{1 - \theta\eta^{1/n}}\,d\eta = -\frac{n}{\theta^{l+1}}\left(\sum_{i=1}^{l}\frac{\theta^i}{i} + \log_e(1-\theta)\right), \qquad \theta < 1,$$

$$l = (k+1)n + j - 1,$$

for all non-negative integer j, k and all positive integer n. Unfortunately, this expression is unsuitable for computational purposes, since it involves the difference of two nearly equal quantities. It may, however, be used to obtain a power series expansion and this was the method used in the computations described in this report. The formulae used for the $J_k(\theta)$ and their derivatives were computed using the formulae

$$J_0(\theta) = \sum_{i=0}^{m}\frac{i\theta^i}{n+i},$$

$$J_1(\theta) = \sum_{i=0}^{m}\frac{n^2\theta^i}{(n+i+1)(2n+i+1)},$$

$$J_1'(\theta) = \sum_{i=0}^{m}\frac{n^2(i+1)\theta^i}{(n+i+2)(2n+i+2)},$$

$$J_2(\theta) = \sum_{i=0}^{m}\frac{2n^3\theta^i}{(n+i+2)(2n+i+2)(3n+i+2)},$$

$$J_2(\theta) = \sum_{i=0}^{m} \frac{2n^3(i+1)\theta^i}{(n+i+3)(2n+i+3)(3n+i+3)},$$

$$J_3(\theta) = \sum_{i=0}^{m} \frac{n^2\theta^i}{(n+i+2)(2n+i+2)},$$

$$J_3'(\theta) = \sum_{i=0}^{m} \frac{n^2(i+1)\theta^i}{(n+i+3)(2n+i+3)},$$

$$J_4(\theta) = \sum_{i=0}^{m} \frac{(i+1)\theta^i}{(n+i+1)},$$

$$J_5(\theta) = \sum_{i=0}^{m} \frac{(i+2)\theta^i}{(n+i+2)},$$

These are truncated series, and the errors involved in using them are bounded by $\frac{n\theta^{m+1}}{1-|\theta|}$; m is selected to ensure that all the errors are less than a predetermined magnitude (in the computations reported here, they were less than 10^{-12}).

While these series give a satisfactory method of computing the integrals $J_k(\theta)$ for power-law profiles, the integrals cannot be expressed in closed form in most other cases. If the correction of Section 3.1 is used for laminar flow, for example, it is necessary to use some kind of quadrature (for example, Simpson's rule) to compute the $J_k(\theta)$.

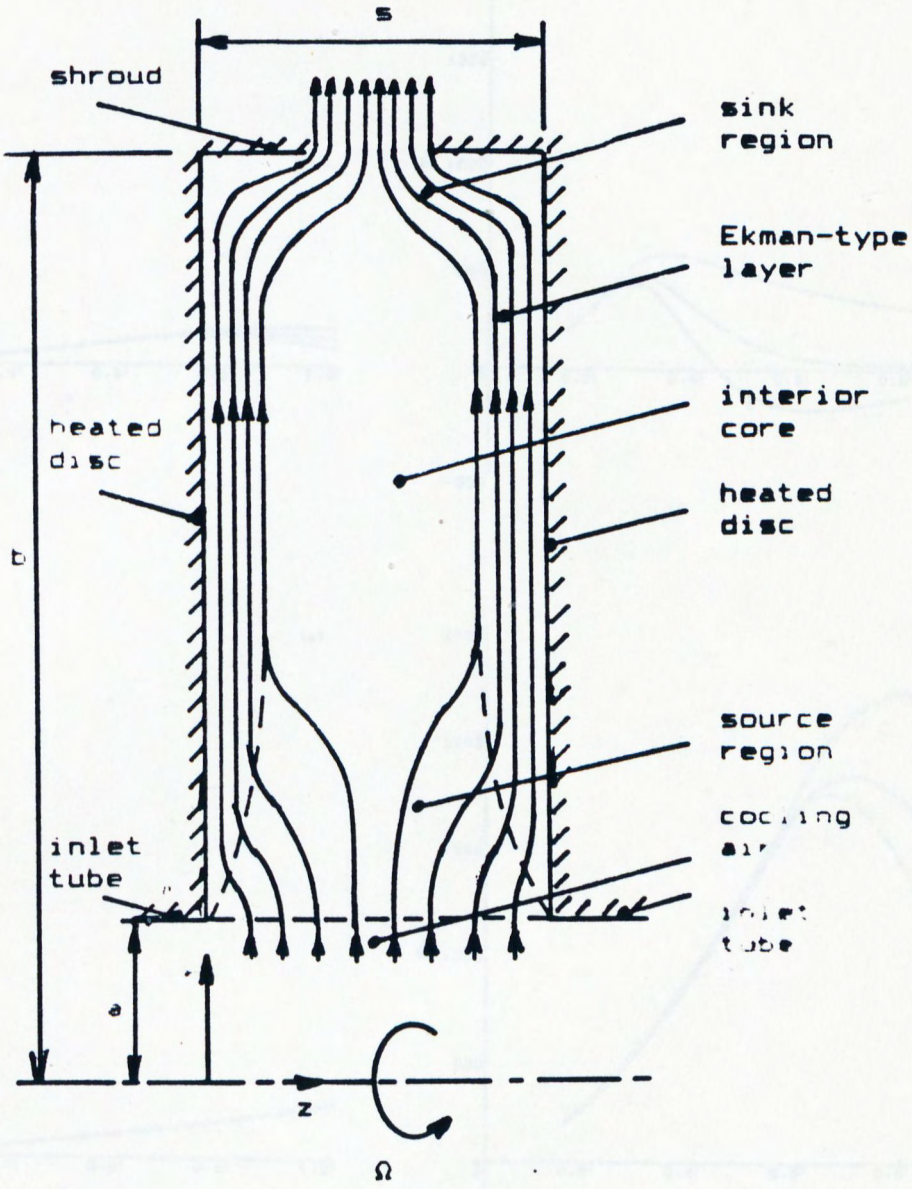

Figure 1 Schematic diagram of flow in the cavity.

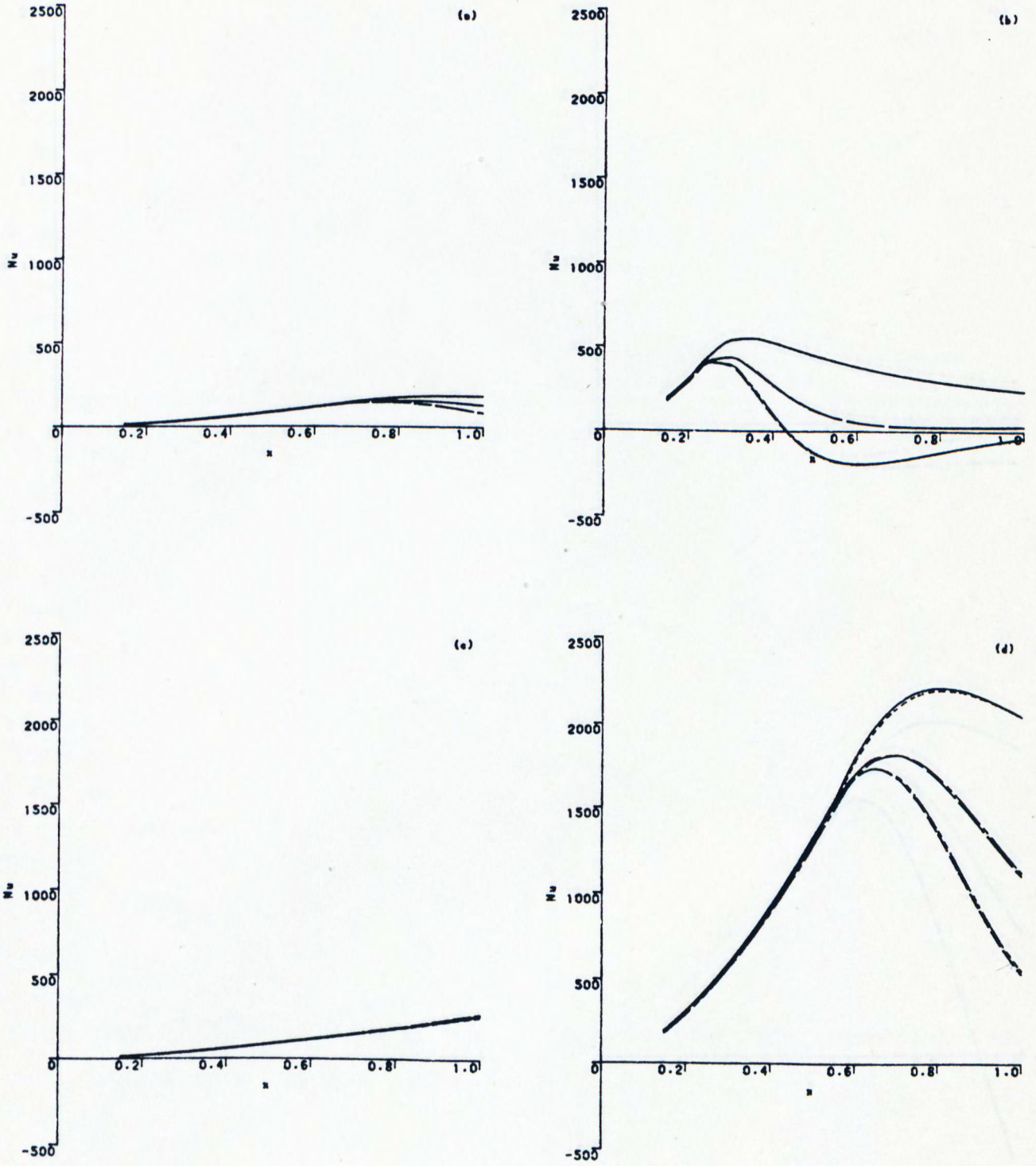

(a) Cw= 1400. Reph:=1E5
(b) Cw= 1400. Reph:=3E6
(c) Cw=14000. Reph:=1E5
(d) Cw=14000. Reph:=3E6
Pr = 1.0
10-JUL-85(11:37) XMDANN

Figure 2 The effect of neglecting axial density gradients.

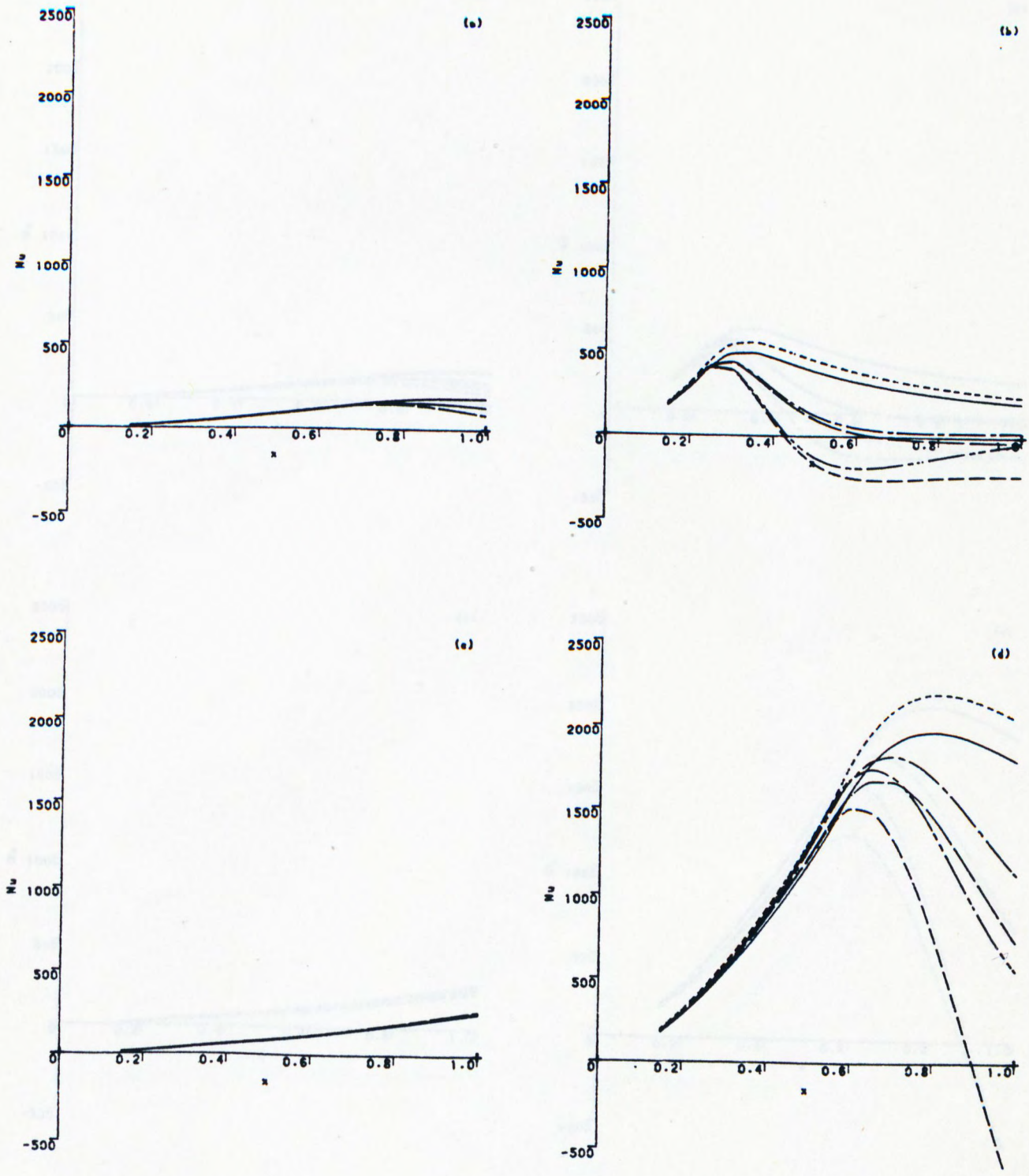

(a) Cw= 1400. Reph:=1E5
(b) Cw= 1400. Reph:=3E6
(c) Cw=14000. Reph:=1E5
(d) Cw=14000. Reph:=3E6
Pr = 1.0
10-JUL-85(17:41) IMDANX

Figure 3 The effect of neglecting viscous dissipation.

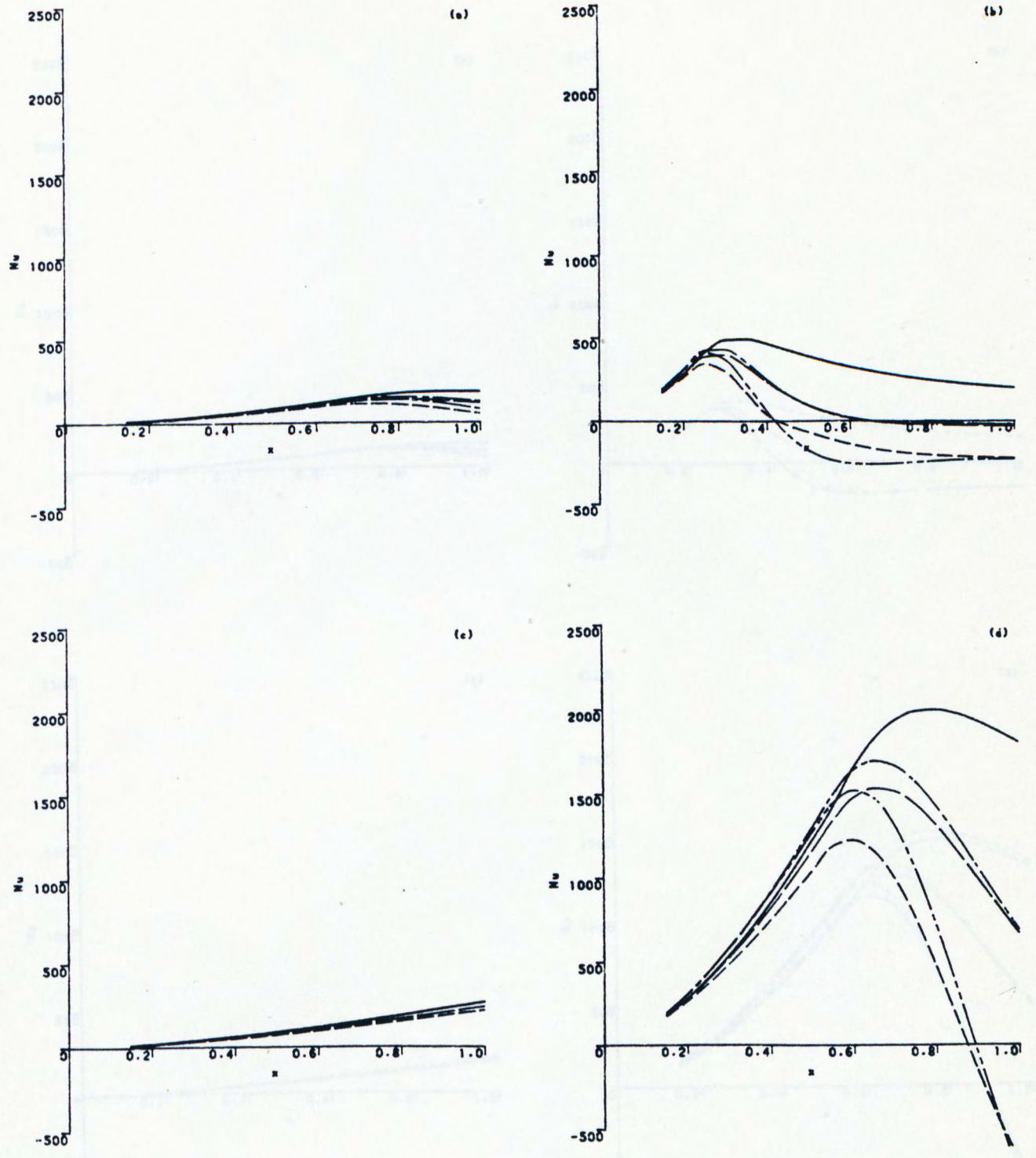

(a) Cw= 1400, Reph:=1E5
(b) Cw= 1400, Reph:=3E6
(c) Cw=14000, Reph:=1E5
(d) Cw=14000, Reph:=3E6
Pr = 1.0
10-JUL-85(18:34) ICDANY

Figure 4 The effect of a nonquadratic disc-temperature distribution on the Reynolds analogy.

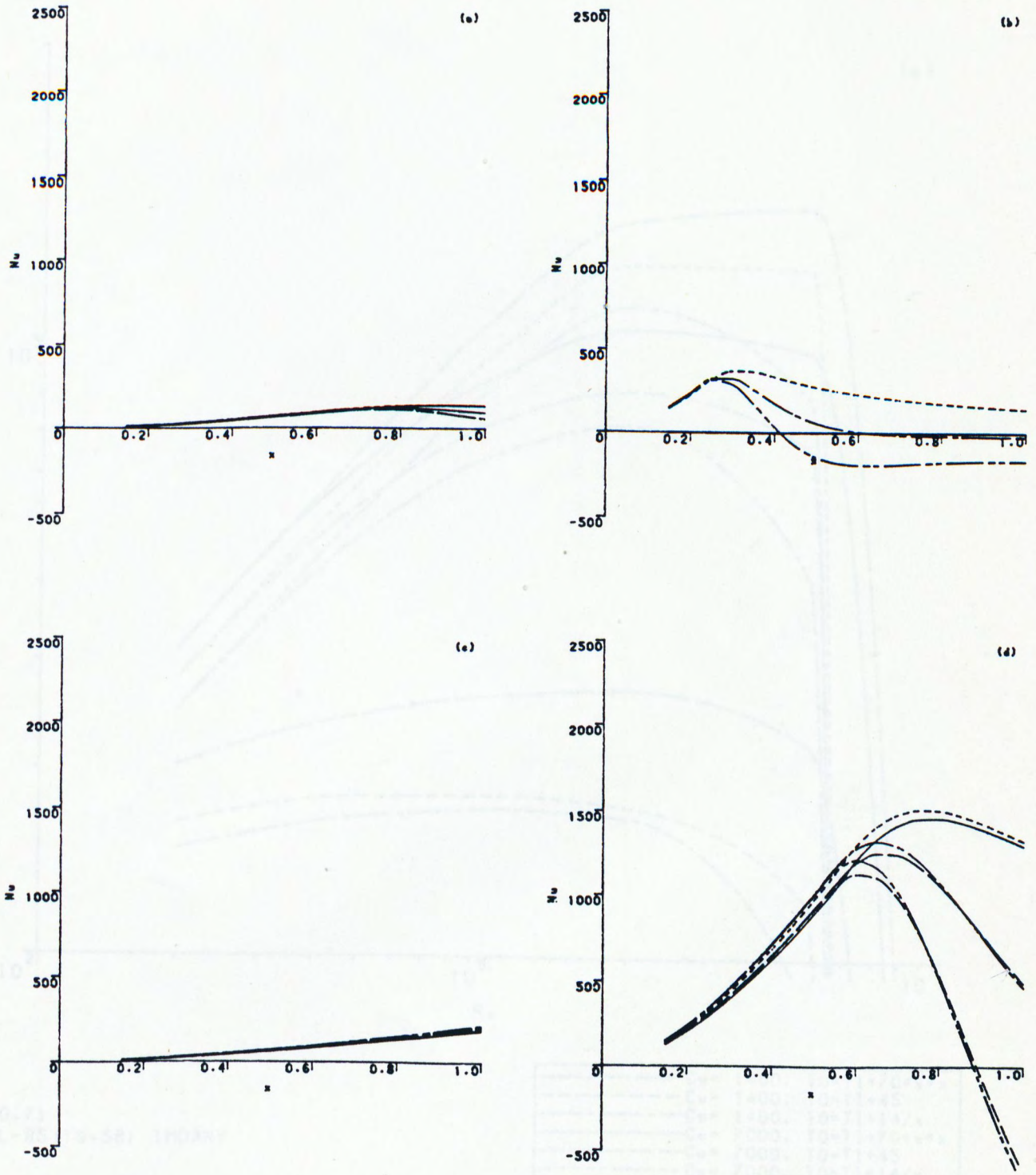

(a) Cw= 1400. Reph:=1E5
(b) Cw= 1400. Reph:=3E6
(c) Cw=14000. Reph:=1E5
(d) Cw=14000. Reph:=3E6
Pr = 0.71
11-JUL-85(19:52) IMDXNY

Figure 5 The effect of using approximations for R and χ.

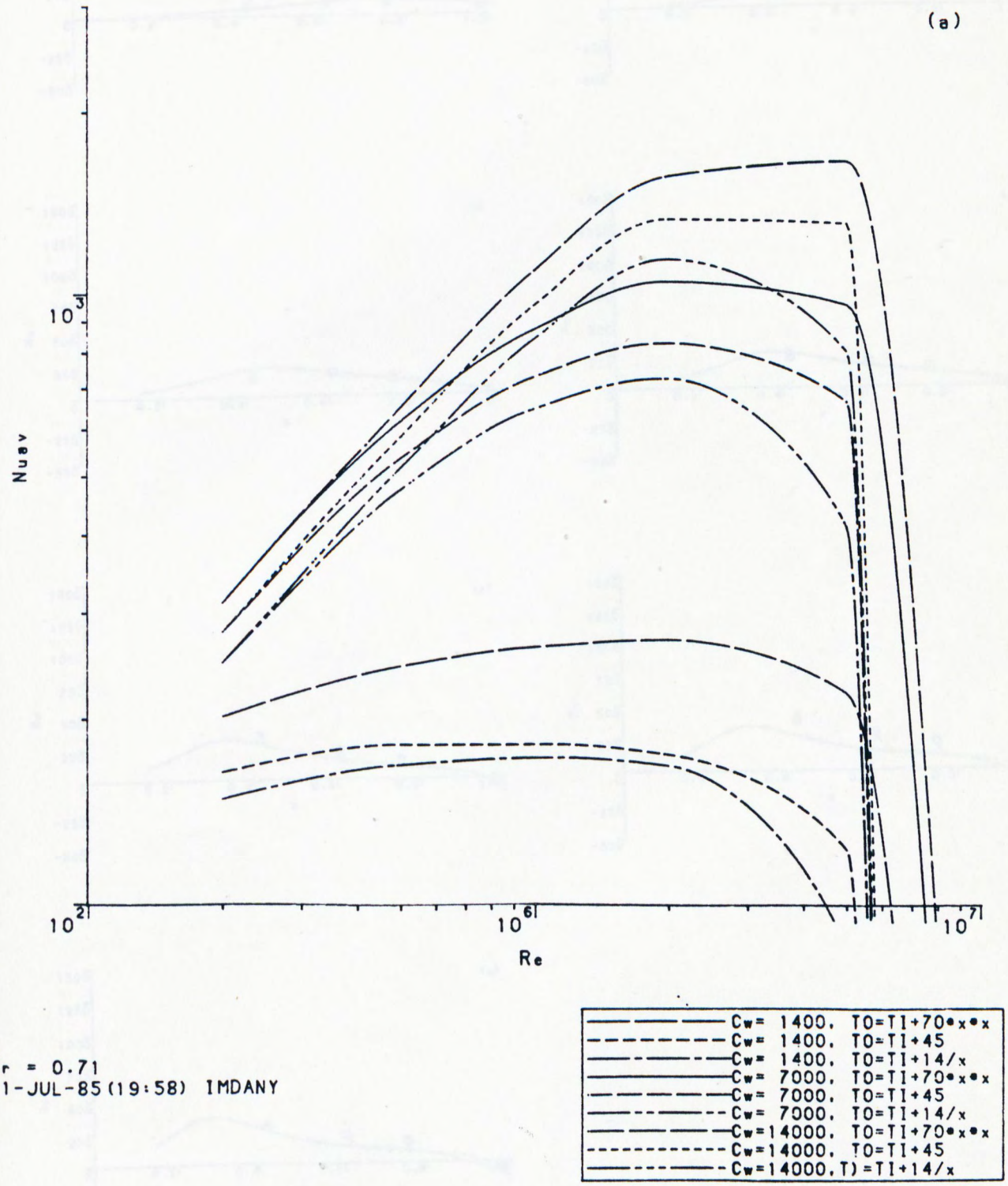

Figure 6 The variation of average Nusselt with Re_x.

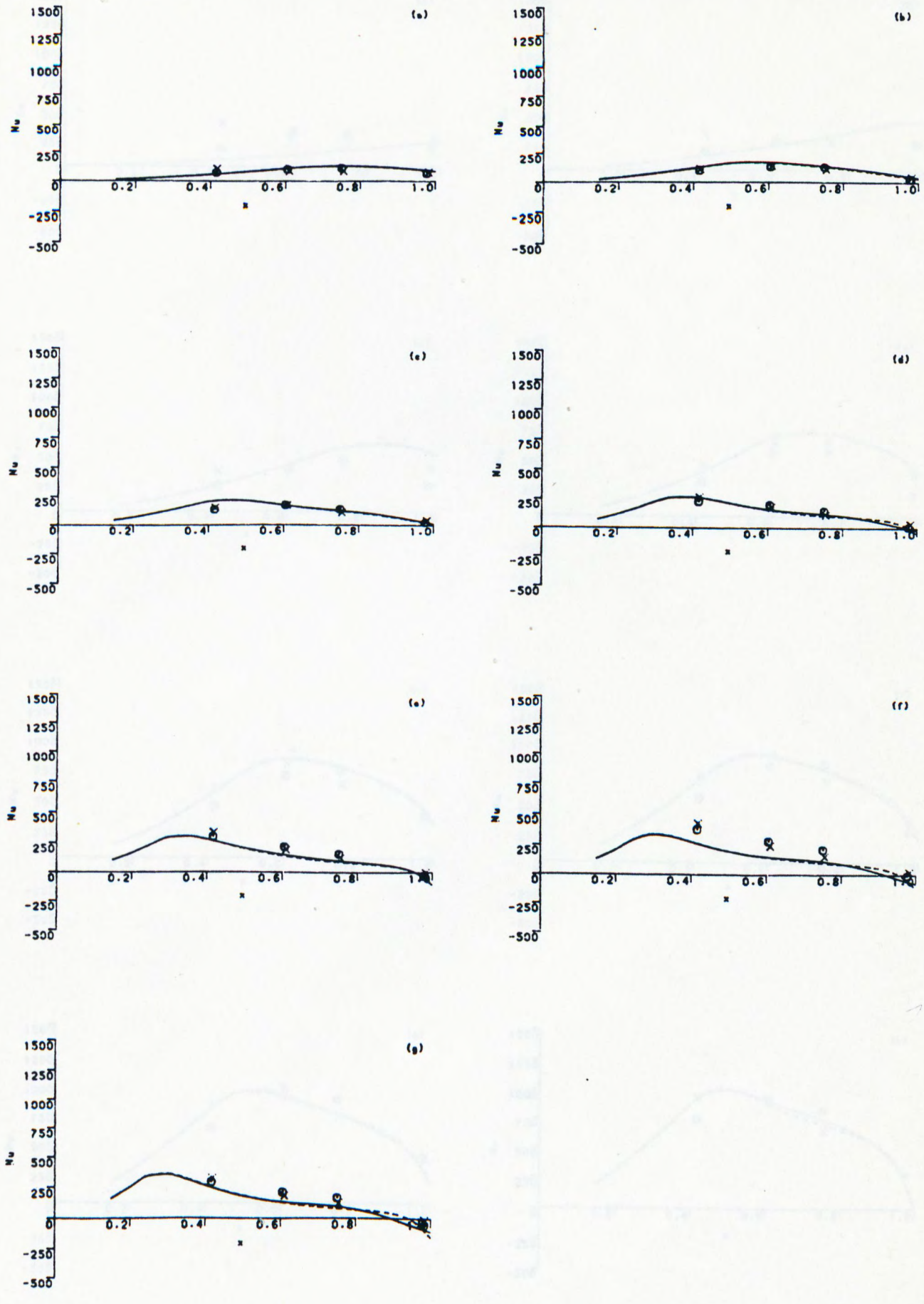

(a) Rephi = 1.33E5 (b) Rephi = 3.30E5
(c) Rephi = 6.62E5 (d) Rephi = 1.24E6
(e) Rephi = 1.87E6 (f) Rephi = 2.48E6
(g) Rephi = 3.12E6

Figure 7 Comparison with experiment. [$C_w = 1400, \frac{dT}{dr} > 0$]

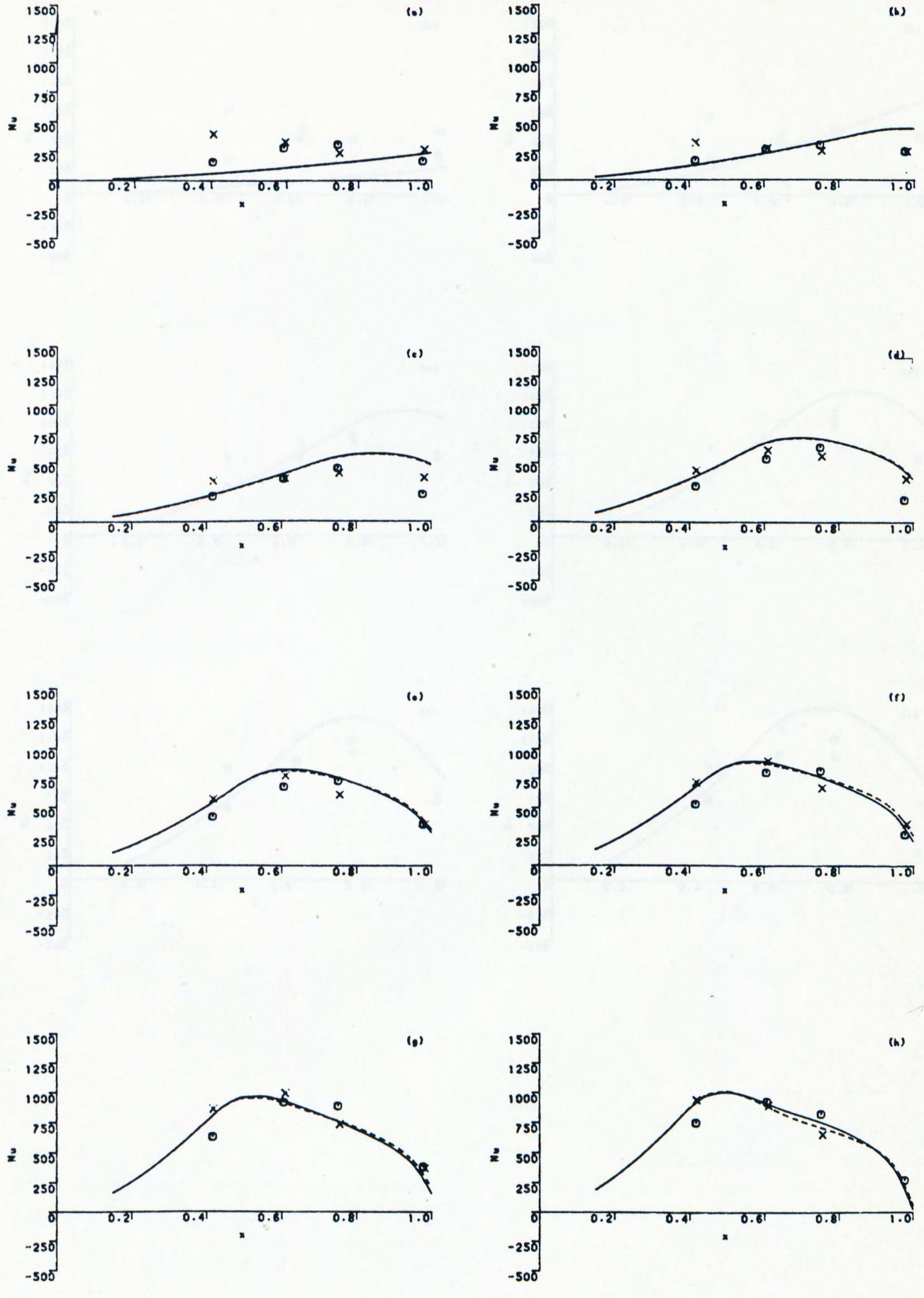

(a) Rephi = 1.25E5 (b) Rephi = 3.29E5
(c) Rephi = 6.50E5 (d) Rephi = 1.30E6
(e) Rephi = 1.96E6 (f) Rephi = 2.58E6
(g) Rephi = 3.22E6 (h) Rephi = 3.95E6

Figure 8 Comparison with experiment. [$C_w = 7000$, $\frac{dT}{dr} > 0$]

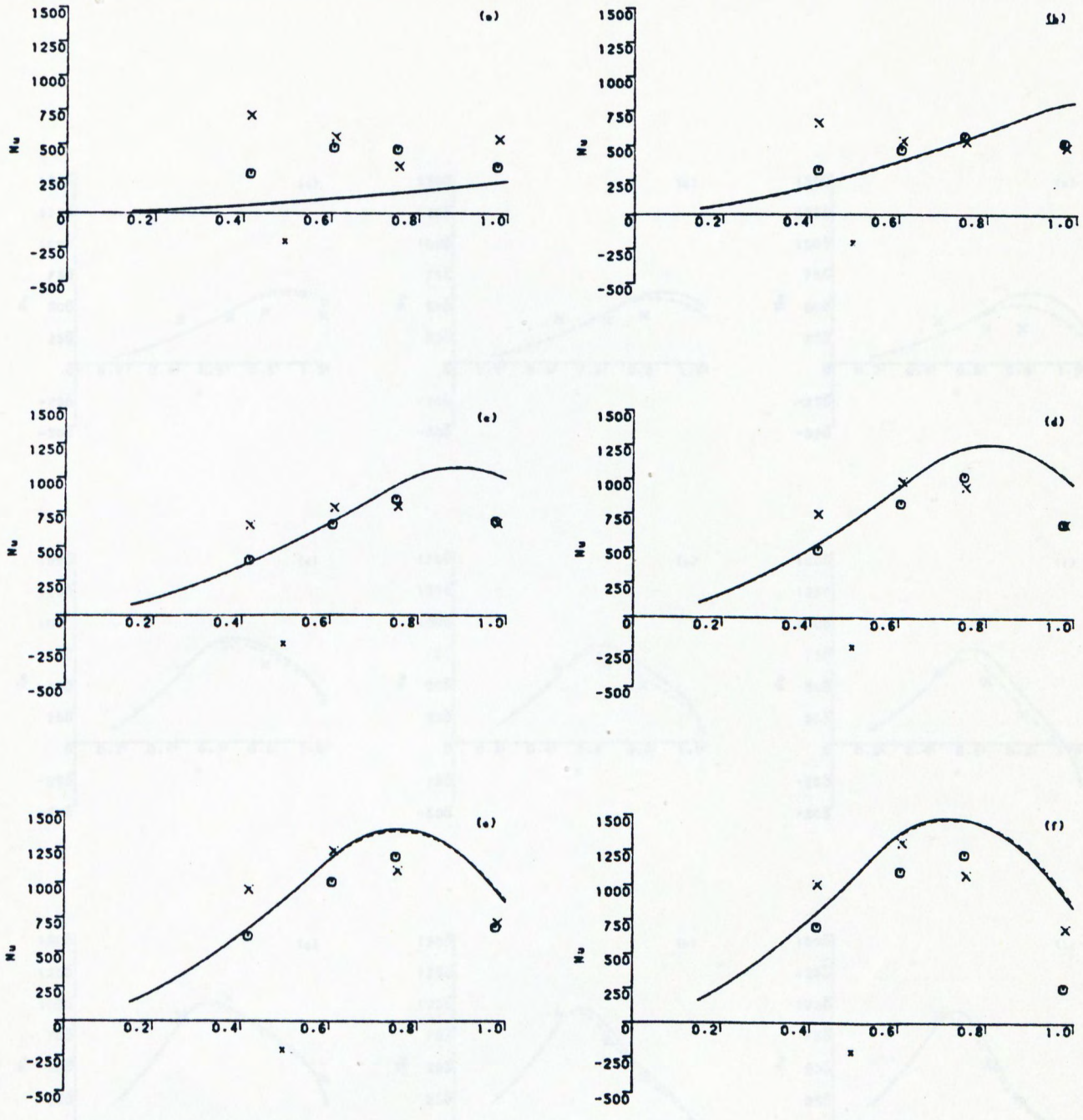

(a) Rephi = 1.22E5 (b) Rephi = 6.08E5
(c) Rephi = 1.24E6 (d) Rephi = 1.90E6
(e) Rephi = 2.52E6 (f) Rephi = 3.18E6

Figure 9 Comparison with experiment. [C_w = 14000, $\frac{dT}{dr} > 0$]

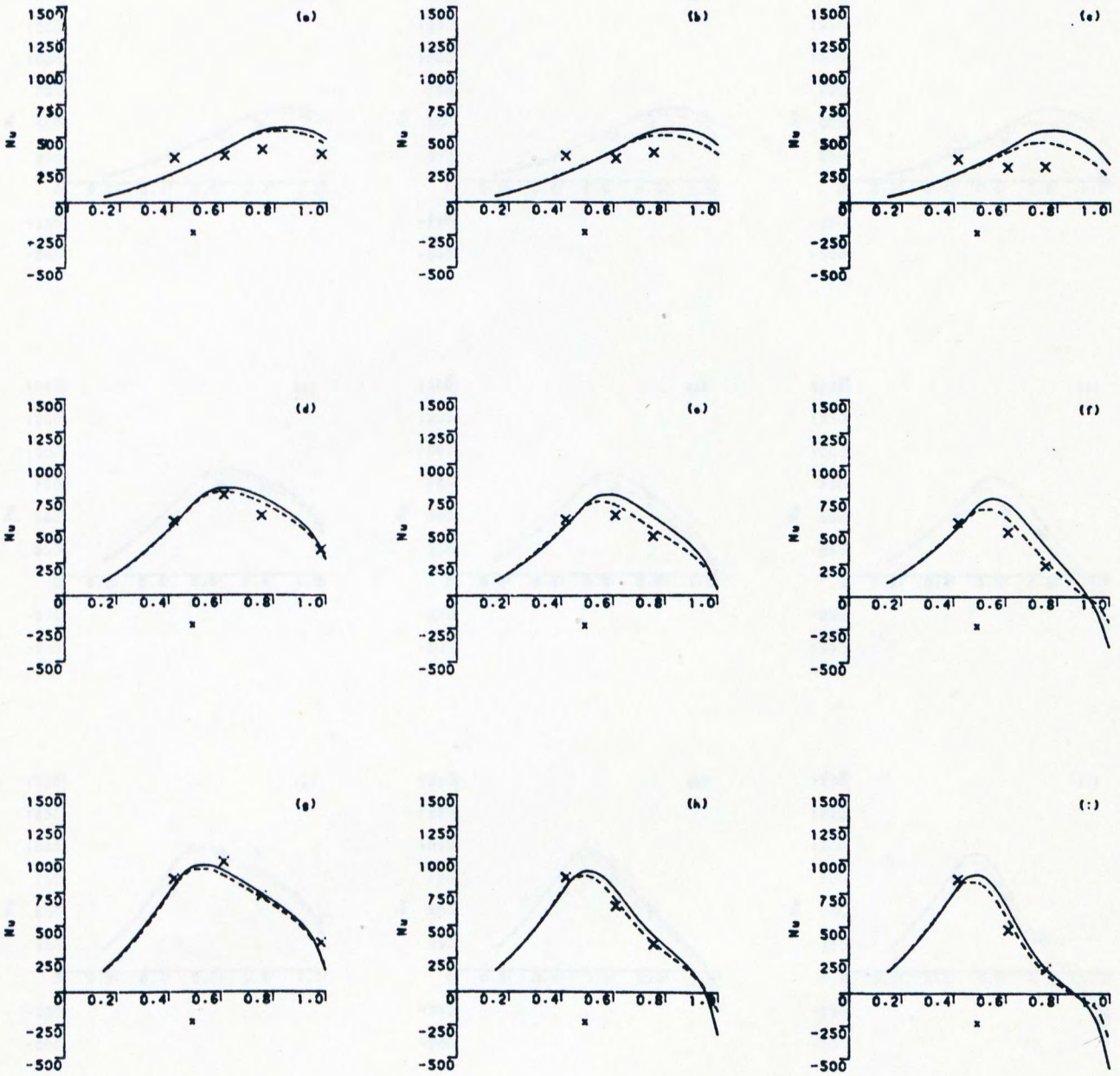

(a) Cw= 7000. Reph:=6.50E5. TO :ncreas:ng
(b) Cw= 7000. Reph:=6.60E5. TO constant
(c) Cw= 7000. Reph:=6.57E5. TO decreas:ng
(d) Cw= 7000. Reph:=1.96E6. TO :ncreas:ng
(e) Cw= 7000. Reph:=1.98E6. TO constant
(f) Cw= 7000. Reph:=1.97E6. TO decreas:ng
(g) Cw= 7000. Reph:=3.22E6. TO :ncreas:ng
(h) Cw= 7000. Reph:=3.26E6. TO constant
(:) Cw= 7000. Reph:=3.29E6. TO decreas:ng
Downstream disc. Pr = 0.71
10-JULY-85(18.51)/IMDAA

Figure 10a Comparison with experiment and Chew's predictions.

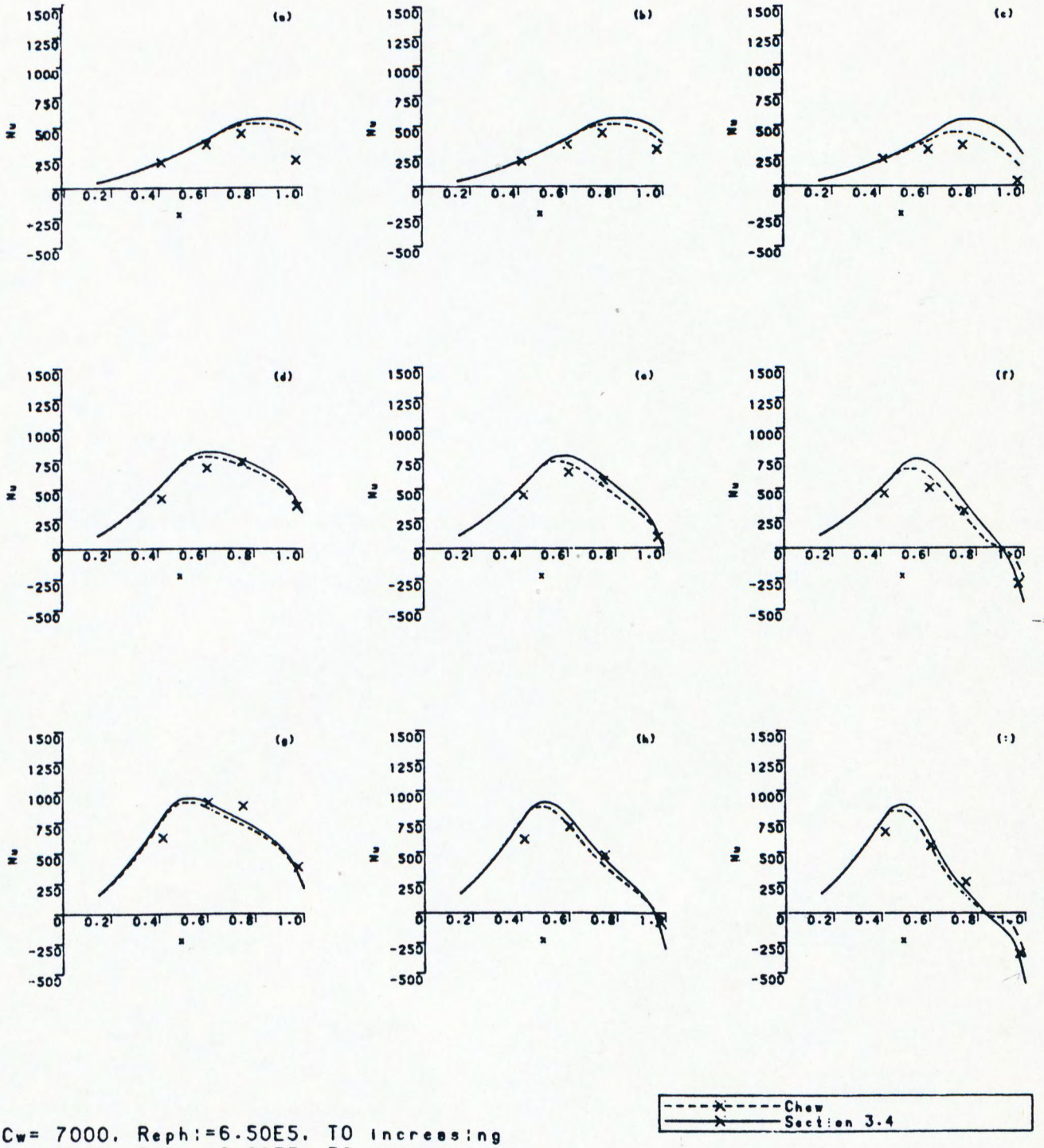

(a) Cw= 7000. Reph:=6.50E5. TO increasing
(b) Cw= 7000. Reph:=6.60E5. TO constant
(c) Cw= 7000. Reph:=6.57E5. TO decreasing
(d) Cw= 7000. Reph:=1.96E6. TO increasing
(e) Cw= 7000. Reph:=1.98E6. TO constant
(f) Cw= 7000. Reph:=1.97E6. TO decreasing
(g) Cw= 7000. Reph:=3.22E6. TO increasing
(h) Cw= 7000. Reph:=3.26E6. TO constant
(i) Cw= 7000. Reph:=3.29E6. TO decreasing
Upstream disc. Pr = 0.71
10-JUL-85(18:51) IMDANY

Figure 10b Comparison with experiment and Chew's predictions.